

# Multiple Layer-Selective Polar Charge Density Waves in EuTe<sub>4</sub>

Wen-Han Dong ,<sup>1</sup> Wenhui Duan ,<sup>1,2,3</sup> Yong Xu ,<sup>1,3,\*</sup> and Peizhe Tang ,<sup>4,5,†</sup>

<sup>1</sup>*State Key Laboratory of Low Dimensional Quantum Physics and Department of Physics, Tsinghua University, Beijing 100084, China*

<sup>2</sup>*Institute for Advanced Study, Tsinghua University, Beijing 100084, China*

<sup>3</sup>*Frontier Science Center for Quantum Information, Beijing, China*

<sup>4</sup>*School of Materials Science and Engineering, Beihang University, Beijing 100191, China*

<sup>5</sup>*Max Planck Institute for the Structure and Dynamics of Matter, Center for Free-Electron Laser Science, 22761 Hamburg, Germany*

EuTe<sub>4</sub> is a polar charge density wave (CDW) material, with giant thermal hysteresis and non-volatile state switching under electric and optical fields, attracting great attention in recent years. However, the in-depth understanding of these anomalous phenomena remains elusive. Herein, via first-principles calculations, we reveal that the polar CDW state in EuTe<sub>4</sub> hosts a novel layer-selective nature, wherein multiple energetically close CDW configurations coexist and exhibit low interconversion energy barriers. Monte Carlo simulations indicate that the giant thermal hysteresis in EuTe<sub>4</sub> originates from a phase transition mainly driven by the change of configurational entropy, around which the material hosts a metastable CDW state characterized by diverse local polar configurations breaking the out-of-plane translational symmetry. The configurational composition of this metastable CDW state can be effectively controlled by electric and optical fields, thereby enabling non-volatile state switching. Our theoretical findings align well with recent experimental observations in EuTe<sub>4</sub> and pave the way for exploring the emerging phenomena and applications of polar CDW in multilayered systems.

*Introduction*—The coexistence and interplay of charge density wave (CDW) [1–3] with other ordered states such as superconductivity, magnetism, and pair density wave have attracted significant interest in the field of condensed matter physics [4–10]. If the point-group or time-reversal symmetries are broken, the CDW states may intertwine with polar or chiral orders, yielding polar or chiral CDWs [11–17]. Among these, polar CDW is a unique platform for exploring the fundamental physics at the intersection of CDW and ferroelectrics. By combining optical tunability [18–21] and ferroelectric controllability [22, 23], polar CDW opens avenues for next-generation optoelectronics and non-volatile memory.

Recently, the multilayered material EuTe<sub>4</sub> has garnered great attention due to the coexistence of CDW and polar orders [24–38]. The unit structure of EuTe<sub>4</sub> comprises a Te monolayer (ML-Te) and a Te bilayer (BL-Te) separated by EuTe layers [see Fig. 1(a)], exhibiting structural anisotropy with different in-plane lattice constants [25]. This material hosts a near-commensurate unidirectional CDW within its Te layers [25–28], which persists up to the transition temperature  $T_{\text{CDW}} \sim 652$  K [35]. The CDW coexists with polar order, as confirmed by second-harmonic generation detection [30]. Interestingly, below  $T_{\text{CDW}}$ , EuTe<sub>4</sub> displays a giant thermal hysteresis in resistance, with a hysteresis loop spanning over 400 K [24–26]. Within the thermal hysteresis loop, the CDW state with polar order can be electrically [29] and optically [30] switched in a non-volatile manner at room tem-

perature, suggesting promising applications of EuTe<sub>4</sub> as efficient memristor [29] and laser-controlled memory [30]. Prior theoretical studies suggest that the observed CDW in EuTe<sub>4</sub> at low temperature is driven by the electron-phonon coupling [25, 34–36]. While, as the temperature increases, the origins of multiple metastable CDW states and rich emergent phenomena—such as giant thermal hysteresis and non-volatile state switching under electric and optical fields—are yet to be well understood. Therefore, the theoretical understanding of the temperature evolution of CDW states in EuTe<sub>4</sub> is urgently needed, which is also crucial for advancing future research and applications of polar CDW.

In this Letter, through density functional theory (DFT) calculations, we reveal that EuTe<sub>4</sub> hosts a novel layer-selective polar CDW as the ground state, where charge density modulations are selectively driven by the *a*-axial polar atomic displacements within both ML-Te and BL-Te. At finite temperature, multiple layer-selective polar CDW configurations coexist in EuTe<sub>4</sub>, which are energetically close due to the relatively weak interlayer couplings between these Te layers and exhibit low interconversion energy barriers. Furthermore, we develop an effective model based on DFT results and perform Monte Carlo (MC) simulations to study the thermal evolution of these CDW configurations. Our simulation results reveal that a metastable CDW state comprising multiple local polar configurations emerges with a configurational-entropy-driven first-order phase transition, thereby leading to a notable thermal hysteresis upon heating and cooling. Electric and optical fields can alter the configurational compositions in such a metastable CDW state, varying its configurational entropy and thus

\* [yongxu@mail.tsinghua.edu.cn](mailto:yongxu@mail.tsinghua.edu.cn)

† [peizhet@buaa.edu.cn](mailto:peizhet@buaa.edu.cn)

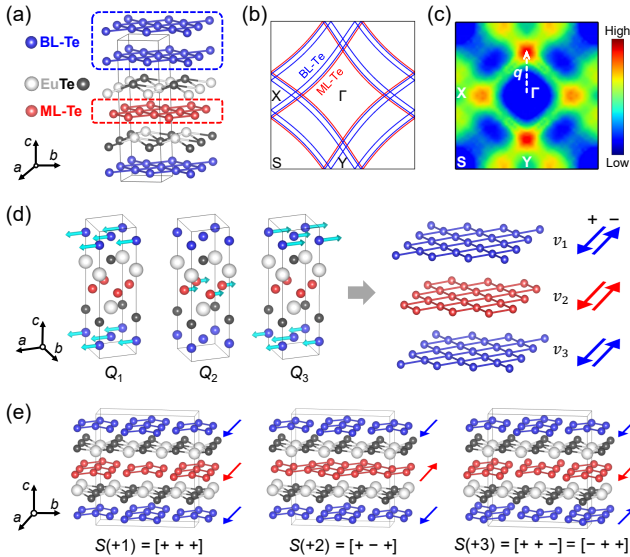


FIG. 1. Multiple layer-selective polar CDW configurations in EuTe<sub>4</sub>. (a) Crystal structure of non-CDW EuTe<sub>4</sub> in *Pmmn* symmetry, showing relatively weak couplings between Te layers. (b) Fermi surface of non-CDW EuTe<sub>4</sub> from tight-binding model. (c) Lindhard function corresponding to (b), exhibiting a dominant peak around  $\mathbf{q} = \frac{1}{3}\mathbf{b}^*$ . (d) Schematics for the imaginary phonons  $Q_{1,2,3}$  at  $\mathbf{q} = \frac{1}{3}\mathbf{b}^*$  (left) and the three-layer CDW representations  $[\nu_1 \nu_2 \nu_3]$  (right), where  $\nu_{1,2,3} = \pm$  describes the polar order of each Te layer. (e) Three nonequivalent  $1 \times 3 \times 1$  CDW configurations with overall positive polarization:  $S(+1)$ ,  $S(+2)$ , and  $S(+3)$ . Their counterparts with negative polarization are  $S(-1) = [---]$ ,  $S(-2) = [-+-]$ , and  $S(-3) = [-+-] = [+--]$ , respectively.

enabling non-volatile state switching. Our work proposes a new mechanism to fully understand recent experimental discoveries in EuTe<sub>4</sub> and opens new avenues for exploring polar CDW in multilayered systems.

*Layer-selective polar CDW*—We begin by elucidating the origin of layer-selective CDW in EuTe<sub>4</sub>. Prior DFT studies reveal that the quasi-2D bands in EuTe<sub>4</sub> around the Fermi level are mainly contributed by ML-Te and BL-Te [34, 36]. To identify the layer contributions to CDW states in EuTe<sub>4</sub>, we construct a tight-binding model considering the intralayer/interlayer interaction inside ML-Te and BL-Te while ignoring the interlayer coupling between them, which well reproduces the DFT electronic structures (see Fig. S1 in Supplemental Material (SM) [39]). Figure 1(b) shows the Fermi surface calculated from the tight-binding model, with overlapping Fermi pockets from ML-Te and BL-Te due to their close on-site energies (Fig. S2 in SM [39]). Influenced by in-plane anisotropy, these Fermi pockets together induce a pronounced unidirectional CDW instability around  $\mathbf{q} = \frac{1}{3}\mathbf{b}^*$  in the Lindhard function [see Fig. 1(c)], matching the experimentally observed  $\mathbf{q}_{\text{CDW}} \sim 0.33\mathbf{b}^*$  [25] and suggesting electron-phonon coupling as the origin of CDW [40]. Layer-resolved Lindhard functions further indicate

that the CDW forms within each Te layer (see Fig. S2 in SM [39]), indicating a layer-selective CDW behavior that accounts for the coexisting CDWs discovered in ML-Te and BL-Te [27, 28]. We highlight the uniqueness of this unidirectional, layer-selective CDW in EuTe<sub>4</sub> in contrast to other rare-earth tellurides, see Sec. III of SM [39].

To understand how polar order emerges from lattice instability in EuTe<sub>4</sub>, we perform DFT calculations to study its phonon spectrum. Consistent with prior calculations [34, 36], we observe the imaginary phonons with lowest frequencies near  $\mathbf{q} = \frac{1}{3}\mathbf{b}^*$  (see Fig. S3 in SM [39]), supporting the Lindhard function results discussed above. Figure 1(d) shows the vibration modes of three imaginary phonons  $Q_{1,2,3}$  at  $\mathbf{q} = \frac{1}{3}\mathbf{b}^*$ . These phonons exhibit *a*-axial (*x*-directional) polar atomic displacements within ML-Te or BL-Te, with  $B_2$  (*x*-polarized) or  $A_2$  (anti-*x*-polarized) irreducible representations of the  $C_{2v}$  little group at  $\mathbf{q} = \frac{1}{3}\mathbf{b}^*$ . Driven by these phonon instabilities, the CDW distortions in EuTe<sub>4</sub> involve specific combinations of polar atomic displacements within each Te layer. Consequently, the CDW in EuTe<sub>4</sub> is concomitant with an *a*-axial polar order in each Te layer [see Fig. 1(d)], underscoring a layer-selective polar CDW feature.

Due to the relatively weak interlayer couplings between Te layers, multiple energetically close, layer-selective polar CDW configurations should coexist in EuTe<sub>4</sub>. Guided by possible combinations of imaginary phonons  $Q_{1,2,3}$ , we employ DFT calculations to identify possible commensurate CDW configurations. As shown in Fig. 1(e), we discover three distinct ferroelectric CDW configurations and their counterparts within the minimal  $1 \times 3 \times 1$  supercell. For simplicity, these unit configurations are abbreviated as  $S(\pm 1)$ ,  $S(\pm 2)$  and  $S(\pm 3)$ , with  $+$  ( $-$ ) denoting an overall polarization along *x* ( $-x$ ) direction. The calculated electric polarizations for these configu-

TABLE I. Nonequivalent  $1 \times 3 \times 2$  CDW configurations, corresponding to the paired configurations for neighboring sites in MC simulations. Here, the linkage "+" means out-of-plane stacking of  $1 \times 3 \times 1$  structural units. The energy is defined per  $1 \times 3 \times 1$  supercell, which contains 6 Eu and 24 Te atoms.

Configuration	$S(+1)+S(+1)$	$S(+2)+S(+2)$	$S(+3)+S(+3)$
Energy (meV)	30.03	37.80	6.72
Configuration	$S(+1)+S(-1)$	$S(+2)+S(-2)$	$S(+3)+S(-3)$
Energy (meV)	<b>0.00</b>	12.36	37.44
Configuration	$S(+1)+S(+2)$	$S(+1)+S(+3)$	$S(+2)+S(+3)$
Energy (meV)	33.00	16.41	21.90
Configuration	$S(+1)+S(-2)$	$S(+1)+S(-3)$	$S(+2)+S(-3)$
Energy (meV)	5.58	17.34	22.17

rations are 2.20, 2.62 and 3.56 ( $\times 10^{-3}$  C/m $^2$ ), respectively [39]. Once we further consider the couplings between structural units and enlarge the supercell along  $z$  direction (i.e.,  $1 \times 3 \times 2$  supercell), all possible low-energy CDW configurations are listed in Table I, which are energetically close (maximal energy difference 1.26 meV/atom), with the antiferroelectric  $S(+1)+S(-1)$  being the ground-state configuration. Notably, these CDW configurations exhibit low interconversion energy barriers ( $< 5.4$  meV/atom), indicating that structural transitions can occur among them as temperature increases and multiple local configurations could coexist in the CDW state below  $T_{CDW}$  (see Fig. S5 in SM [39]).

*Effective model for MC simulations*—To simulate the thermal effects associated with multiple energetically close CDW configurations in EuTe<sub>4</sub>, we develop a 1D effective model based on the low-energy approximation, see Sec. IV of SM [39]. In this model, each unit site corresponds to a  $1 \times 3 \times 1$  supercell that adopts one possible CDW configuration among  $S(\pm 1)$ ,  $S(\pm 2)$ , and  $S(\pm 3)$  [see Fig. 2(a)], with probabilities determined by their relative energies and temperature. We assume the polarization of each CDW configuration is temperature-independent, while thermal fluctuations only affect the system's entropy, further influencing the statistical distribution of local configurations.

Along the out-of-plane direction, the whole system has  $N$  sites, described by a global CDW state  $\mathbf{S} = [S_1 \ S_2 \ \dots \ S_{N-1} \ S_N]$ . Each site  $i$  hosts a local configuration  $S_i$  with polarization  $\mathbf{P}(S_i)$ , and couples to adjacent sites via nearest-neighbor interactions  $D(S_i, S_{i\pm 1})$  [see Fig. 2(b)]. The averaged Landau-Devonshire internal energy  $U(\mathbf{S})$  [41, 42] is:

$$U(\mathbf{S}) = \frac{1}{N} \sum_i^N \left\{ \frac{A(S_i)}{2} \mathbf{P}^2(S_i) + \frac{B(S_i)}{4} \mathbf{P}^4(S_i) + \frac{C(S_i)}{6} \mathbf{P}^6(S_i) + \frac{D(S_i, S_{i\pm 1})}{2} (\mathbf{P}(S_i) - \mathbf{P}(S_{i\pm 1}))^2 \right\}, \quad (1)$$

where the first three terms describe the polarization-contributed energy within each site, and the last term captures inter-site interactions between neighboring sites. The local polarization  $\mathbf{P}(S_i)$  and parameters  $A(S_i)$ ,  $B(S_i)$ ,  $C(S_i)$  and  $D(S_i, S_{i\pm 1})$  are fitted from DFT calculations (see Tables S1 and S2 in SM [39]). Since the global CDW state could host multiple local configurations, we introduce the averaged Helmholtz free energy  $H(\mathbf{S})$  to include entropy contributions [43]:

$$H(\mathbf{S}) = U(\mathbf{S}) - TS_{\text{config}}, \quad S_{\text{config}} = -k_B \sum_{\mathbb{C}} n_{\mathbb{C}} \ln \left( \frac{n_{\mathbb{C}}}{N_{\mathbb{C}}} \right). \quad (2)$$

Here,  $T$  is temperature.  $S_{\text{config}}$  is configurational entropy, while the effect of vibrational entropy is estimated to be

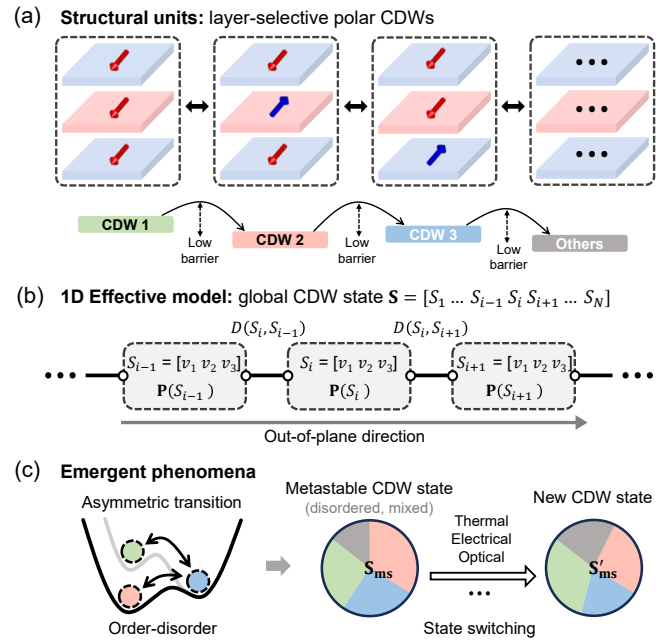


FIG. 2. Framework for understanding EuTe<sub>4</sub>-like systems. (a) Multiple layer-selective polar CDW configurations with low interconversion energy barriers. (b) Schematic for the effective model, where each site hosts one  $1 \times 3 \times 1$  CDW configuration among  $S(\pm 1)$ ,  $S(\pm 2)$ , and  $S(\pm 3)$ . (c) Schematics for the underlying order-disorder physics (left) and non-volatile state switching (right). The balls depict various possible paired configurations, while fan areas show their populations in the metastable CDW state.

negligible, see Sec. V of SM [39].  $k_B$  is Boltzmann constant.  $n_{\mathbb{C}}$  is the population of each possible paired configuration for two neighboring sites [see Table I]. In a 1D model with  $N$  sites, there are  $N$  paired configurations in total.  $N_{\mathbb{C}}$  is the degeneracy for each paired configuration, where  $N_{\mathbb{C}} = 4$  for the pairs with  $S(+3)+S(\pm 3)$ ,  $N_{\mathbb{C}} = 2$  for that with  $S(+1)+S(\pm 3)$  and  $S(+2)+S(\pm 3)$ , and  $N_{\mathbb{C}} = 1$  for others. Note that this definition of  $S_{\text{config}}$  inherently includes contributions from all possible stacking configurations.

Having established the effective model, we proceed to explore thermal effects in EuTe<sub>4</sub> using MC simulations, see computational details in SM [39]. At zero temperature, the system adopts an ordered, antiferroelectric ground state  $\mathbf{S}_g$ , in which any neighboring sites exhibit a paired configuration as  $S(+1)+S(-1)$ . As temperature increases, thermal excitation can transform the local paired configurations in  $\mathbf{S}_g$  into other ones with close energies [see Fig. 2(c)], inducing a metastable CDW state  $\mathbf{S}_{\text{ms}}$  that breaks translation symmetry along the out-of-plane direction. Hereafter, our MC simulations will substantiate the thermally driven  $\mathbf{S}_{\text{ms}}$  in EuTe<sub>4</sub> and illustrate that the properties of  $\mathbf{S}_{\text{ms}}$  are controllable thermally, electrically, and optically, yielding rich emergent phenomena as depicted in Fig. 2(c).

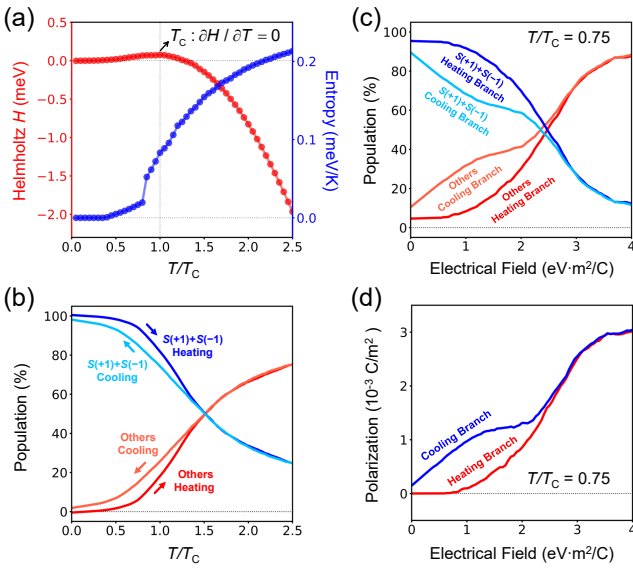


FIG. 3. Thermal hysteresis and electrical state control. (a) Temperature-dependent Helmholtz free energy  $H(\mathbf{S})$  (red) and configurational entropy  $S_{\text{config}}$  (blue), obtained from *average-mode* MC simulations [39]. Here, the temperature ( $T$ ) is normalized by critical temperature ( $T_C$ ). (b) Population ratios of the ground-state paired configuration ( $S(+1)+S(-1)$ ) versus other configurations ("Others") upon heating and (then) cooling, obtained from *heating-cooling-mode* MC simulations [39] with a sweep rate of  $|\delta(T/T_C)| = 5.0 \times 10^{-3}$ . (c) Population ratios of paired configurations and (d) polarization under a  $x$ -directional electric field, obtained from *average-mode* MC simulations [39] and initialized from the heating and cooling branches of (b) at  $T/T_C = 0.75$ . In (b-d), the curves are smoothed to reduce fluctuations.

**MC simulation results**—We first simulate the thermal behavior of  $\text{EuTe}_4$  to uncover the underlying physical origin for the giant thermal hysteresis observed experimentally [24–26]. Figure 3(a) presents the temperature dependence of  $H(\mathbf{S})$  and  $S_{\text{config}}$ . Below the critical value  $T_C$ ,  $H(\mathbf{S})$  and  $S_{\text{config}}$  slightly increase with temperature as the system accumulates CDW fluctuations deviating from the ground state to gradually accommodate compositional disorder (see Fig. S7 in SM [39]). Upon approaching  $T_C$ ,  $H(\mathbf{S})$  decreases gradually and  $S_{\text{config}}$  increases sharply, indicating a first-order order-disorder phase transition in  $\text{EuTe}_4$  [43]. This phase transition reflects the melting of the ordered  $\mathbf{S}_g$  into  $\mathbf{S}_{\text{ms}}$ , which contains diverse local configurations with layer-selective polar CDW at high temperature. To reveal the thermal hysteresis resulting from this first-order phase transition, we simulate the thermal evolution of the global CDW state in a heating-cooling cycle initiated from  $\mathbf{S}_g$ , while tracking the change of populations for the ground-state paired configuration and other configurations. Our results show a notable thermal hysteresis loop centered around  $T_C$  [see Fig. 3(b) and Fig. S8 in SM [39]]. To distinguish  $\mathbf{S}_{\text{ms}}$  in different thermal branches, we de-

note them as  $\mathbf{S}_{\text{ms}}^h$  and  $\mathbf{S}_{\text{ms}}^c$  for the heating and cooling branches, respectively. At a given temperature,  $\mathbf{S}_{\text{ms}}^h$  and  $\mathbf{S}_{\text{ms}}^c$  have different distributions of local CDW configurations, which could contribute to resistance differently. Hence, we expect the experimentally observed thermal hysteresis in resistance [24–26] to have the same physical origin as the hysteresis discussed here. Thus, our findings promise to resolve the long-standing debate about the origin of the giant thermal hysteresis in  $\text{EuTe}_4$  and provide a new perspective on the thermal hysteresic phenomena in CDW materials beyond known mechanisms, such as impurity pinning [44], sliding stacking order [45], metal-to-insulator transition [46], and CDW transitions across wave vectors [47, 48].

Within the thermal hysteresis loop, the CDW state in  $\text{EuTe}_4$  can be manipulated electrically [29]. To study the switching of  $\mathbf{S}_{\text{ms}}$  under a static electric field  $\mathbf{E}$ , we incorporate the electric-field-polarization coupling term  $-\frac{1}{N} \sum_i^N \mathbf{E} \cdot \mathbf{P}(S_i)$  [42] into  $H(\mathbf{S})$  in Eq. 2. Figure 3(c) shows an efficient electrical control of  $\mathbf{S}_{\text{ms}}$  at  $T/T_C = 0.75$ , where a notable difference persists between  $\mathbf{S}_{\text{ms}}^h$  and  $\mathbf{S}_{\text{ms}}^c$  [see Fig. 3(b)]. Under an increasing electric field, the switching of  $\mathbf{S}_{\text{ms}}$  occurs smoothly, indicating a continuous reorganization of the system's local polar configurations, as also reflected by the non-linear, gradual increase of polarization in Fig. 3(d). This finding provides essential insights into the smooth, non-volatile electrical switching of resistance observed in  $\text{EuTe}_4$  [29], confirming that its metastable CDW states consist of numerous local polar configurations, thereby producing electrically controllable free-energy landscapes. Furthermore, Fig. 3(d) shows that, under a relatively low electric field ( $< 2.2 \text{ eV} \cdot \text{m}^2/\text{C}$ ), the cooling branch exhibits larger polarization than the heating branch, revealing the energy storage during thermal hysteresis in  $\text{EuTe}_4$  and suggesting promising electrocaloric applications [49–51].

Inspired by experimental observations of photoinduced

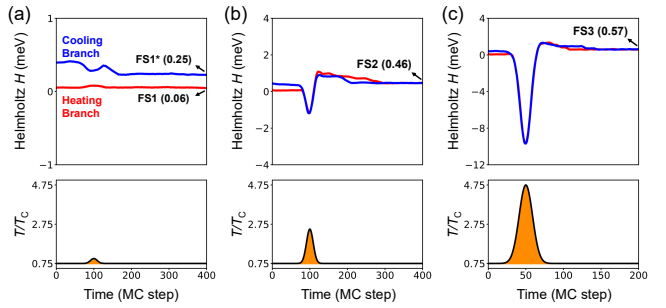


FIG. 4. Optical state control. (a) MC-simulated evolution of  $H(\mathbf{S})$  (upper) under a Gaussian heat pulse with amplitude of 0.25 (bottom). (b) and (c) display the results under pulse amplitudes of 1.75 and 4, respectively. In (a-c), the curves are smoothed and are initialized from the heating and cooling branches of Fig. 3(b) at  $T/T_C = 0.75$ . FS\* denote the final states, with their  $H(\mathbf{S})$  shown in parentheses.

long-lived metastable CDW states in  $\text{EuTe}_4$  [30], we investigate the optical control of  $\mathbf{S}_{\text{ms}}$ . Since the observed features of equilibrium states are insensitive to light polarization and coherence [30], we conclude the optical pumping as a photoinduced thermal effect and simulate the optical fields via the Gaussian heat pulses. Figure 4 shows that, at  $T/T_C = 0.75$ , the photoinduced modulations of  $\mathbf{S}_{\text{ms}}^h$  and  $\mathbf{S}_{\text{ms}}^c$  can be tuned by varying the pulse strength. When we apply a weak pumping pulse, final states [FS1 and FS1\* in Fig. 4(a)] remain close to their unpumped states. As we increase the pumping strength, a relatively strong pulse first thermally excites  $\mathbf{S}_{\text{ms}}^h$  and  $\mathbf{S}_{\text{ms}}^c$  into high- $S_{\text{config}}$  states, after which they relax to similar final states [FS2 in Fig. 4(b)]. Once we further enhance the pumping strength, new final states with higher  $H(\mathbf{S})$  [FS3 in Fig. 4(c)] can be achieved. We propose a physical picture for these optical processes in Fig. S10 of SM [39], suggesting that photoinduced thermal effects can significantly tailor the system's hysteresis behavior, enabling hidden metastable CDW states that are inaccessible via thermal excitation. Our simulations illuminate the underlying mechanism to explain the pulse-dependent, non-volatile optical state switching in  $\text{EuTe}_4$  [30], which would guide non-volatile memory applications in this and similar CDW materials.

*Conclusion*—Our first-principles calculations identify  $\text{EuTe}_4$  as a layer-selective polar CDW material, in which multiple energetically close CDW configurations coexist around the ground state. Our MC simulations reveal that, as temperature increases, thermal excitation could alter the distribution of local paired CDW configurations and enhance the configurational entropy. Hence, a first-order phase transition can be achieved and result in a notable thermal hysteresis upon heating and cooling, which could promisingly resolve the long-standing debate about the origin of giant thermal hysteresis in  $\text{EuTe}_4$ . Within the thermal hysteresis loop, we further demonstrate that the  $\mathbf{S}_{\text{ms}}$  can be effectively controlled under electric and optical fields, aligning with recent observations of non-volatile switching of CDW states in  $\text{EuTe}_4$  [29, 30] and underscoring its promising applications in non-volatile memory [30], memristors [52], thermoelectrics [32], and electrocalorics [49–51]. Our work not only clarifies the essential nature of CDW states in  $\text{EuTe}_4$ , but also establishes a general framework for exploring a new class of polar CDW in multilayered systems.

*Acknowledgments*—We thank Dong Wu, Tao Dong, Qiaomei Liu and Jin Zhang for helpful discussions. This work was supported by the Basic Science Center Project of NSFC (Grant No. 52388201), the National Natural Science Foundation of China (Grants No. 12334003, No. 12421004, No. 12361141826, No. 12234011, No. 12374053 and No. 12504078), the National Science Fund for Distinguished Young Scholars (Grant No. 12025405), the National Key Basic Research and Development Program of China (Grants No. 2023YFA1406400 and No.

2024YFA1409100), the Innovation Program for Quantum Science and Technology (Grant No. 2023ZD0300500). The work was carried out at the National Supercomputer Center in Tianjin using the Tianhe new generation supercomputer.

---

[1] X. Zhu, Y. Cao, J. Zhang, E. W. Plummer, and J. Guo, *Proc. Natl. Acad. Sci.* **112**, 2367 (2015).

[2] L. P. Gor'kov and G. Grüner, *Charge density waves in solids*, Vol. 25 (Elsevier, 2012).

[3] K. Rossnagel, *J. Phys. Condens. Mat.* **23**, 213001 (2011).

[4] E. Fradkin, S. A. Kivelson, and J. M. Tranquada, *Rev. Mod. Phys.* **87**, 457 (2015).

[5] X. Liu, Y. X. Chong, R. Sharma, and J. S. Davis, *Science* **372**, 1447 (2021).

[6] S. D. Wilson and B. R. Ortiz, *Nat. Rev. Mater.* **9**, 420 (2024).

[7] K. Jiang, T. Wu, J.-X. Yin, Z. Wang, M. Z. Hasan, S. D. Wilson, X. Chen, and J. Hu, *Nat. Sci. Rev.* **10**, nwac199 (2022).

[8] X. Teng, L. Chen, F. Ye, E. Rosenberg, Z. Liu, J.-X. Yin, Y.-X. Jiang, J. S. Oh, M. Z. Hasan, K. J. Neubauer, *et al.*, *Nature* **609**, 490 (2022).

[9] Y. Wang, H. Wu, G. T. McCandless, J. Y. Chan, and M. N. Ali, *Nat. Rev. Phys.* **5**, 635 (2023).

[10] H. Chen, H. Yang, B. Hu, Z. Zhao, J. Yuan, Y. Xing, G. Qian, Z. Huang, G. Li, Y. Ye, *et al.*, *Nature* **599**, 222 (2021).

[11] Y. Zhang, H. X. Yang, C. Ma, H. F. Tian, and J. Q. Li, *Phys. Rev. Lett.* **98**, 247602 (2007).

[12] J. van Wezel, *Phys. Rev. B* **85**, 035131 (2012).

[13] G. Liu, T. Qiu, K. He, Y. Liu, D. Lin, Z. Ma, Z. Huang, W. Tang, J. Xu, K. Watanabe, *et al.*, *Nat. Nanotechnol.* **18**, 854 (2023).

[14] S. Wu, F.-T. Huang, X. Xu, E. T. Ritz, T. Birol, S.-W. Cheong, and G. Blumberg, *Nat. Commun.* **15**, 9276 (2024).

[15] J. Ishioka, Y. H. Liu, K. Shimatake, T. Kurosawa, K. Ichimura, Y. Toda, M. Oda, and S. Tanda, *Phys. Rev. Lett.* **105**, 176401 (2010).

[16] G. Li, H. Yang, P. Jiang, C. Wang, Q. Cheng, S. Tian, G. Han, C. Shen, X. Lin, H. Lei, *et al.*, *Nat. Commun.* **13**, 2914 (2022).

[17] X. Song, L. Liu, Y. Chen, H. Yang, Z. Huang, B. Hou, Y. Hou, X. Han, H. Yang, Q. Zhang, *et al.*, *Nat. Commun.* **13**, 1843 (2022).

[18] G. Grüner, *Rev. Mod. Phys.* **60**, 1129 (1988).

[19] I. Vaskivskyi, I. Mihailovic, S. Brazovskii, J. Gospodaric, T. Mertelj, D. Svetin, P. Sutar, and D. Mihailovic, *Nat. Commun.* **7**, 11442 (2016).

[20] A. Zong, X. Shen, A. Kogar, L. Ye, C. Marks, D. Chowdhury, T. Rohwer, B. Freelon, S. Weathersby, R. Li, *et al.*, *Sci. Adv.* **4**, eaau5501 (2018).

[21] A. Kogar, A. Zong, P. E. Dolgirev, X. Shen, J. Straquadrine, Y.-Q. Bie, X. Wang, T. Rohwer, I.-C. Tung, Y. Yang, *et al.*, *Nat. Phys.* **16**, 159 (2020).

[22] C. Wang, L. You, D. Cobden, and J. Wang, *Nat. Mater.* **22**, 542 (2023).

[23] D. Zhang, P. Schoenherr, P. Sharma, and J. Seidel, *Nat. Rev. Mater.* **8**, 25 (2023).

[24] Q. Q. Zhang, Y. Shi, K. Y. Zhai, W. X. Zhao, X. Du, J. S. Zhou, X. Gu, R. Z. Xu, Y. D. Li, Y. F. Guo, *et al.*, *Phys. Rev. B* **107**, 115141 (2023).

[25] D. Wu, Q. M. Liu, S. L. Chen, G. Y. Zhong, J. Su, L. Y. Shi, L. Tong, G. Xu, P. Gao, and N. L. Wang, *Phys. Rev. Mater.* **3**, 024002 (2019).

[26] B. Q. Lv, A. Zong, D. Wu, A. V. Rozhkov, B. V. Fine, S.-D. Chen, M. Hashimoto, D.-H. Lu, M. Li, Y.-B. Huang, *et al.*, *Phys. Rev. Lett.* **128**, 036401 (2022).

[27] B. Q. Lv, A. Zong, D. Wu, Z. Nie, Y. Su, D. Choi, B. Ilyas, B. T. Fichera, J. Li, E. Baldini, *et al.*, *Phys. Rev. Lett.* **132**, 206401 (2024).

[28] B. Q. Lv, Y. Su, A. Zong, Q. Liu, D. Wu, N. F. Yuan, Z. Nie, J. Li, S. Sarker, S. Meng, *et al.*, *Nat. Mater.* **24**, 1 (2025).

[29] R. Venturini, M. Rupnik, J. Gašperlin, J. Lipič, P. Šutar, Y. Vaskivskyi, F. Šćepanović, D. Grabnar, D. Golež, and D. Mihailovic, *arXiv:2412.13094* (2024).

[30] Q. Liu, D. Wu, T. Wu, S. Han, Y. Peng, Z. Yuan, Y. Cheng, B. Li, T. Hu, L. Yue, *et al.*, *Nat. Commun.* **15**, 8937 (2024).

[31] C. Zhang, Q.-Y. Wu, Y.-H. Yuan, X. Zhang, H. Liu, Z.-T. Liu, H.-Y. Zhang, J.-J. Song, Y.-Z. Zhao, F.-Y. Wu, *et al.*, *Phys. Rev. B* **106**, L201108 (2022).

[32] H. Takahashi, K. Yoshida, A. Nakano, and S. Ishiwata, *PRX Energy* **4**, 033009 (2025).

[33] K. H. Oh, Y. Su, H. Ning, B. Q. Lv, A. Zong, D. Wu, Q. Liu, G. Kang, H. Choi, H.-W. J. Kim, *et al.*, *arXiv:2509.16493* (2025).

[34] K. Xiao, W.-H. Dong, X. Wang, J. Yu, D. Fu, Z. Hu, Y. Guo, Q. Zhang, X. Hou, Y. Guo, *et al.*, *Nano Lett.* **24**, 7681 (2024).

[35] R. Rathore, A. Pathak, M. K. Gupta, R. Mittal, R. Kulkarni, A. Thamizhavel, H. Singhal, A. H. Said, and D. Bansal, *Phys. Rev. B* **107**, 024101 (2023).

[36] A. Pathak, M. K. Gupta, R. Mittal, and D. Bansal, *Phys. Rev. B* **105**, 035120 (2022).

[37] H. Ning, K. H. Oh, Y. Su, Z. D. Shi, D. Wu, Q. Liu, B. Q. Lv, A. Zong, G. Kang, H. Choi, *et al.*, *Phys. Rev. Lett.* **135**, 246504 (2025).

[38] R. Rathore, H. Singhal, V. Dwij, M. K. Gupta, A. Pathak, J. A. Chakera, R. Mittal, A. P. Roy, A. Babu, R. Kulkarni, *et al.*, *Ultrafast Sci.* **3**, 0041 (2023).

[39] See Supplemental Material for details about: I. Computational methods; II. Origin of layer-dependent polar CDW; III. Distinctions between EuTe<sub>4</sub> and other *RTen*; IV. DFT energy data and low-energy approximation; V. Negligible influence of vibrational entropy; and VI. MC simulations for CDW states, which includes Refs. [53–72].

[40] M. D. Johannes and I. I. Mazin, *Phys. Rev. B* **77**, 165135 (2008).

[41] R. Fei, W. Kang, and L. Yang, *Phys. Rev. Lett.* **117**, 097601 (2016).

[42] V. L. Ginzburg, *Phys.-Uspekhi* **44**, 1037 (2001).

[43] D. Frenkel, *Physica A* **263**, 26 (1999).

[44] C. S. Lue, Y.-K. Kuo, F. H. Hsu, H. H. Li, H. D. Yang, P. S. Fodor, and L. E. Wenger, *Phys. Rev. B* **66**, 033101 (2002).

[45] S.-H. Lee, J. S. Goh, and D. Cho, *Phys. Rev. Lett.* **122**, 106404 (2019).

[46] X. Granados, J. Fontcuberta, X. Obradors, and J. B. Torrance, *Phys. Rev. B* **46**, 15683 (1992).

[47] S. Wall, B. Krenzer, S. Wippermann, S. Sanna, F. Klasing, A. Hanisch-Blicharski, M. Kammler, W. G. Schmidt, and M. Horn-von Hoegen, *Phys. Rev. Lett.* **109**, 186101 (2012).

[48] P.-J. Hsu, T. Mauerer, M. Vogt, J. J. Yang, Y. S. Oh, S.-W. Cheong, M. Bode, and W. Wu, *Phys. Rev. Lett.* **111**, 266401 (2013).

[49] F. Du, T. Yang, H. Hao, S. Li, C. Xu, T. Yao, Z. Song, J. Shen, C. Bai, R. Luo, *et al.*, *Nature* **640**, 924 (2025).

[50] H. Qi, L. Chen, S. Deng, and J. Chen, *Nat. Rev. Mater.* **8**, 355 (2023).

[51] X. Qian, D. Han, L. Zheng, J. Chen, M. Tyagi, Q. Li, F. Du, S. Zheng, X. Huang, S. Zhang, *et al.*, *Nature* **600**, 664 (2021).

[52] M. Lanza, S. Pazos, F. Aguirre, A. Sebastian, M. Le Gallo, S. M. Alam, S. Ikegawa, J. J. Yang, E. Vianello, M.-F. Chang, *et al.*, *Nature* **640**, 613 (2025).

[53] G. Kresse and J. Furthmüller, *Phys. Rev. B* **54**, 11169 (1996).

[54] J. P. Perdew, K. Burke, and M. Ernzerhof, *Phys. Rev. Lett.* **77**, 3865 (1996).

[55] G. Henkelman, B. P. Uberuaga, and H. Jónsson, *J. Chem. Phys.* **113**, 9901 (2000).

[56] S. Grimme, J. Antony, S. Ehrlich, and H. Krieg, *J. Chem. Phys.* **132**, 154104 (2010).

[57] J. B. Neaton, C. Ederer, U. V. Waghmare, N. A. Spaldin, and K. M. Rabe, *Phys. Rev. B* **71**, 014113 (2005).

[58] H. Yao, J. A. Robertson, E.-A. Kim, and S. A. Kivelson, *Phys. Rev. B* **74**, 245126 (2006).

[59] V. Brouet, W. L. Yang, X. J. Zhou, Z. Hussain, R. G. Moore, R. He, D. H. Lu, Z. X. Shen, J. Laverock, S. B. Dugdale, *et al.*, *Phys. Rev. B* **77**, 235104 (2008).

[60] R. Dronskowski and P. E. Bloechl, *J. Phys. Chem.* **97**, 8617 (1993).

[61] V. L. Deringer, A. L. Tchougréeff, and R. Dronskowski, *J. Phys. Chem. A* **115**, 5461 (2011).

[62] N. Marzari and D. Vanderbilt, *Phys. Rev. B* **56**, 12847 (1997).

[63] A. A. Mostofi, J. R. Yates, Y.-S. Lee, I. Souza, D. Vanderbilt, and N. Marzari, *Comput. Phys. Commun.* **178**, 685 (2008).

[64] K. Y. Shin, V. Brouet, N. Ru, Z. X. Shen, and I. R. Fisher, *Phys. Rev. B* **72**, 085132 (2005).

[65] K. Yumigeta, Y. Qin, H. Li, M. Blei, Y. Attarde, C. Kopas, and S. Tongay, *Adv. Sci.* **8**, 2004762 (2021).

[66] K. Y. Shin, J. Laverock, Y. Q. Wu, C. L. Condron, M. F. Toney, S. B. Dugdale, M. J. Kramer, and I. R. Fisher, *Phys. Rev. B* **77**, 165101 (2008).

[67] S. Bhowal and N. A. Spaldin, *Annu. Rev. Mater. Res.* **53**, 53 (2023).

[68] A. Togo, *J. Phys. Soc. Jpn.* **92**, 012001 (2023).

[69] A. Togo and I. Tanaka, *Scr. Mater.* **108**, 1 (2015).

[70] J. Brookeman and A. Rigamonti, *Phys. Rev. B* **24**, 4925 (1981).

[71] B. Y. Sukharevskii, V. Ksenofontov, V. Kovarskii, A. Ul'yanov, and I. Vilkova, *Sov. Phys. JETP* **60**, 767 (1984).

[72] S. Kartha, J. A. Krumhansl, J. P. Sethna, and L. K. Wickham, *Phys. Rev. B* **52**, 803 (1995).